Inorg. Chem. **2006**, *45*, 10576–10584

Electronic Transitions Involved in the Absorption Spectrum and Dual Luminescence of Tetranuclear Cubane [Cu_4I_4(pyridine)$_4$] Cluster: a Density Functional Theory/Time-Dependent Density Functional Theory Investigation

Filippo De Angelis,*,† Simona Fantacci,† Antonio Sgamellotti,† Elena Cariati,‡ Renato Ugo,‡ and Peter C. Ford§

Istituto CNR di Scienze e Tecnologie Molecolari, c/o Dipartimento di Chimica, Università degli studi di Perugia, via Elce di Sotto, 8, I-60123 Perugia, Italy, Dipartimento di Chimica Inorganica, Metallorganica e Analitica dell'Università di Milano and Unità di Ricerca ISTM di Milano, via Venezian 21, I-20133 Milano, Italy, and Department of Chemistry and Biochemistry, University of California, Santa Barbara, California 93106-9510

Received June 23, 2006

We present a combined density functional theory (DFT)/time-dependent density functional theory (TDDFT) study of the geometry, electronic structure, and absorption and emission properties of the tetranuclear "cubane" $Cu_4I_4py_4$ (py = pyridine) system. The geometry of the singlet ground state and of the two lowest triplet states of the title complex were optimized, followed by TDDFT excited-state calculations. This procedure allowed us to characterize the nature of the excited states involved in the absorption spectrum and those responsible for the dual emission bands observed for this complex. In agreement with earlier experimental proposals, we find that while in absorption the halide-to-pyridine charge-transfer excited state (XLCT*) has a lower energy than the cluster-centered excited state (CC*), a strong geometrical relaxation on the triplet cluster-centered state surface leads to a reverse order of the excited states in emission.

Introduction

Multinuclear compounds of copper(I) and other coinage metals have attracted considerable interest, due to their unusual structural and photoluminescence properties.[1] In particular, cuprous iodide and pyridine-based ligands provide remarkable structural diversity depending on their stoichiometry: for a 1:1:1 Cu:I:L (L = pyridine-like ligand) ratio, the most common structural motif is the tetranuclear cubane cluster,[2] even though for L = pyridine a polymeric stair arrangement has been also characterized.[3] Different structural motifs have been reported for stoichiometric ratios 1:1:2 and 1:1:3.[4,5] Recently, some of us have identified new structural motifs of CuI adducts with η^1-nitrogen donor pseudoaromatic [para-substituted pyridines or (*E*)-stilbazoles] ligands, which have raised considerable interest due to their sometimes unusual emissive behavior and structurally dependent second-order nonlinear optical properties.[6] Among the various Cu−I−L clusters, the photophysical properties of the tetranuclear [$Cu_4X_4py_4$] compounds (X = halide, py = pyridine) have been extensively investigated due to their peculiar photoluminescence properties.[1,7] In particular, the title [$Cu_4I_4py_4$]

* To whom correspondence should be addressed. E-mail: filippo@thch.unipg.it.
† Istituto CNR di Scienze e Tecnologie Molecolari.
‡ Università di Milano and Unità di Ricerca ISTM di Milano.
§ University of California.

(1) (a) Ford, P. C.; Cariati, E.; Bourassa, J. *Chem. Rev.* **1999**, *99*, 3625. (b) Omary, M. A.; Mohamed, A. A.; Rawashdeh-Omary, M. A.; Fackler, J. P. *Coord. Chem. Rev.* **2005**, *249*, 1372−1381. (c) Dias, H. V. R.; Diyabalanage, H. V. K.; Eldabaja, M. G.; Elbjeirami, O.; Rawashdeh-Omary, M. A.; Omary, M. A. *J. Am. Chem. Soc.* **2005**, *127*, 7489−7501. (d) Lo, W.-Y.; Lam, C.-H.; Yam, V. W.-W.; Zhu, N.; Cheung, K.-K.; Fathallah, S.; Messaoudi, S.; Le Guennic, B.; Kahlal, S.; Halet, J.-F. *J. Am. Chem. Soc.* **2004**, *126*, 7300−7310.
(2) Raston, C. L.; White, A. H. *J. Chem. Soc., Dalton Trans.* **1976**, 2153.
(3) Eitel, E.; Oelkrug, D.; Hiller, W.; Strahle, J. *Z. Naturforsch.* **1980**, *35b*, 1247.
(4) Rath, N. P.; Maxwell, J. L.; Holt, E. M. *J. Chem. Soc., Dalton Trans.* **1986**, 2449.
(5) Dyason, J. C.; Healy, P. C.; Pakawatchai, C.; Patrick, V. A.; White, A. H. *Inorg. Chem.* **1985**, *24*, 1957.
(6) (a) Cariati, E.; Roberto, D.; Ugo, R.; Ford, P. C.; Galli, S.; Sironi, A. *Inorg. Chem.* **2005**, *44*, 4077. (b) Cariati, E.; Roberto, D.; Ugo, R.; Ford, P. C.; Galli, S.; Sironi, A. *Chem. Mater.* **2002**, *14*, 5116.
(7) Vitale, M.; Ryu, K. C.; Ford, P. C. *Inorg. Chem.* **1993**, *32*, 869.

10.1021/ic061147f CCC: $33.50
Published on Web 11/23/2006

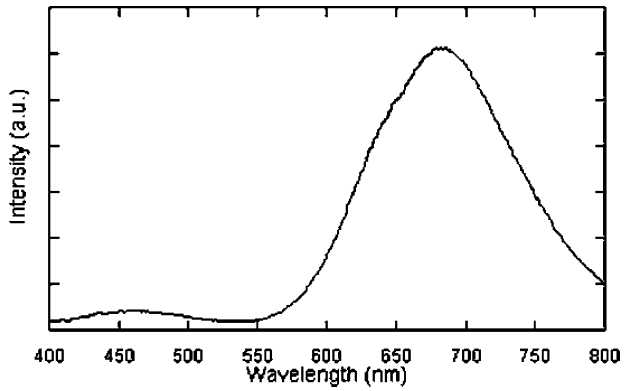

Figure 1. Room-temperature emission spectrum of $[Cu_4I_4py_4]$ in toluene ($\lambda^{exc} = 330$ nm).

complex displays two distinct emission bands[8−10] with a marked environmental sensitivity and with relative intensities that vary with excitation source and sharply with temperature. The low-energy (LE) band dominates at room temperature while the high-energy (HE) band becomes more prominent at low temperatures. This temperature dependence of the emission spectra of $[Cu_4I_4py_4]$ was first noted by Hardt and co-workers,[11] who coined the term "luminescent thermochromism". After this pioneering work, experimental investigations on the interesting luminescence behavior of tetranuclear Cu(I) complexes have been reported by Vogler and Kunkely,[12] Henary and Zink,[13] Holt and co-workers,[14] Oelkrug and co-workers,[15] and Yam et al.,[16] consistently pointing at the HE emission as involving the ligands' π^* orbitals and the LE emission as involving Cu−I cluster delocalized orbitals.

The room-temperature emission spectrum of $[Cu_4I_4py_4]$ in toluene solution is displayed in Figure 1 and is the same as that reported by Kyle et al.[8] Not only does this show two emission bands with maxima at 460 and 690 nm, but time-resolved luminescence studies have demonstrated that these two bands decay with markedly different lifetimes. The lifetime of the lower-energy emission is 10.6 μs under these conditions, while for the higher-energy emission it is 450 ns. Furthermore, the excitation profiles for these two bands are different and display the interesting anomaly that the excitation maximum for the higher-energy emission occurs at longer wavelength than that for the lower-energy band. The theme of multiple emissions that are uncoupled is common for such tetrahedral clusters as well as a number of other coinage metal clusters,[1,9] and this photophysical behavior has been attributed to the presence of several excited states similar in energy but having different orbital parentages.[1] In these cases, the distortions of the excited states, relative to the ground state, occur along different coordinates. As a result, internal conversion from one excited state to another involves substantial nuclear motion and, for this reason, is slow.

On the basis of the available experimental evidence,[1] the low-energy emission band, with λ_{max} at 690 nm, was attributed to a triplet Cu−I cluster-centered (^{3}CC) excited state with the excitation localized to the Cu_4I_4 core. The high-energy band, measured here at 460 nm, was tentatively assigned as emission from a triplet halide-to-pyridine ligand charge-transfer (^{3}XLCT) excited state. Early theoretical investigations by Vitale el al.[17,18] performed on $[Cu_4I_4py_4]$ have contributed to the understanding of the ground-state electronic structure of this species and provided some support for the assigned nature of these excited states by means of ΔSCF calculations, in which excited-state energies are obtained as the differences between the total energies of two Slater determinants corresponding to different electronic configurations. In those studies, however, geometry optimizations were not performed either for the ground state or for the excited states, so that an accurate calculation of the excited states involved in the absorption and emission processes would provide better insight into these processes.

Here we present a full density functional theory (DFT)/time-dependent density functional theory (TDDFT) investigation of the geometry, electronic structure, and optical properties of $[Cu_4I_4py_4]$ aimed at providing a definitive characterization of the photophysical properties of this system. We optimized the geometry of the singlet ground state and of the two lowest triplet states by means of DFT calculations. On the optimized geometries we performed TDDFT calculations of several singlet and triplet states; thus we have gained detailed insight about the electronic origin of the absorption and emission properties.

Previous theoretical investigations on related tetranuclear Cu(I) compounds have been limited to the ground state,[19] while ab initio calculations[20] and more recently TDDFT calculations[21,22] on mononuclear Cu(I) complexes have been reported.

Experimental Section

Computational Details. All the calculations have been performed with the Gaussian03 (G03) program package.[23] The B3LYP

(8) Kyle, K. R.; Ryu, C. K.; DiBenedetto, J. A.; Ford, P. C. *J. Am. Chem. Soc.* **1991**, *113*, 2954.
(9) Ford, P. C.; Vogler, A. *Acc. Chem. Res.* **1993**, *26*, 220.
(10) Ford, P. C. *Coord. Chem. Rev.* **1994**, *132*, 129.
(11) (a) Hardt, H. D.; Pierre, A. *Z. Anorg. Allg. Chem.* **1973**, *402*, 107. (b) Hardt, H. D.; Stoll, H.-J. *Z. Anorg. Allg. Chem.* **1981**, *480*, 193. (c) Hardt, H. D.; Stoll, H.-J. *Z. Anorg. Allg. Chem.* **1981**, *480*, 199.
(12) Vogler, A.; Kunkely, H. *J. Am. Chem. Soc.* **1986**, *108*, 7211.
(13) Henary, M.; Zink, J. I. *J. Am. Chem. Soc.* **1989**, *111*, 7407.
(14) (a) Rath, N. P.; Holt, E. M.; Tanimura, K. *Inorg. Chem.* **1985**, *24*, 3934. (b) Rath, N. P.; Holt, E. M.; Tanimura, K. *J. Chem. Soc., Dalton Trans.* **1986**, 2303.
(15) (a) Radjaipour, M.; Oelkrug, D. *Ber. Bunsen-Ges. Phys. Chem.* **1978**, *82* 159. (b) Eitel, E.; Oelkrug, D.; Hiller, W. J.; Strähle, J. *Z. Naturforsch.* **1980**, *35b*, 1247.
(16) (a) Yam, V. W.-W.; Lee, W.-K.; Cheung, K.-K. *J. Chem. Soc., Dalton Trans.* **1996**, 2335. (b) Yam, V. W.-W.; Lam, C.-H.; Zhu, N. *Inorg. Chim. Acta* **2002**, *331*, 239.
(17) Vitale, M.; Palke, W. E.; Ford, P. C. *J. Phys. Chem.* **1992**, *96*, 8329.
(18) Vitale, M.; Ryu, K. C.; Palke, W. E.; Ford, P. C. *Inorg. Chem.* **1994**, *33*, 561.
(19) Vega, A.; Saillard, J.-Y. *Inorg. Chem.* **2004**, *43*, 4012.
(20) Simon, J. A.; Palke, W. E.; Ford, P. C. *Inorg. Chem.* **1996**, *35*, 6413.
(21) Waterland, M. R.; Howell, S. L.; Gordon, K. C.; Burrell, A. K. *J. Phys. Chem. A* **2005**, *109*, 8826.
(22) Yang, L.; Feng, J.-K.; Ren, A.-M.; Zhang, M.; Ma, Y.-G. Ma, Liu, X.-D. *Eur. J. Inorg. Chem.* **2005**, 1867.

exchange-correlation functional[24] was used throughout. A LANL2DZ basis set[25] was used for all the atoms, along with the corresponding pseudopotential for Cu and I atoms.[26] The same basis set was used for both geometry optimizations and TDDFT calculations. To check the effect of basis set expansion and quality on the calculated geometrical structures and optical properties, geometry optimization of the singlet ground state and TDDFT calculation of the lowest four singlet−singlet and singlet−triplet excitation energies were calculated with a larger basis set composed by 6-311G* for Cu[27] and I[28] and 6-31G* for C, N, and H atoms,[29] respectively. Indeed, it has been recently shown that bond distances in d^{10} complexes can be quite sensitive to the presence of polarization functions in the basis set.[30] For Cu, N, C, and H atoms we used the basis sets contained in the G03 library, while the 6-311G* basis set for I was downloaded from the EMSL basis set library.[31] All the calculations have been performed under D_{2d} symmetry constraints. To check the effect of symmetry lowering, we performed additional geometry optimizations of the singlet ground state using C_{2v} and C_2 symmetry constraints and checked the resulting minima by performing frequency calculations. Geometry optimizations of the two lowest triplet states were performed at the SCF level considering different starting molecular orbital occupations (guess = alter keyword in G03); see the discussion in a later section. In the calculation of the optical absorption spectrum, the 120 lowest spin-allowed singlet−singlet transitions, up to an energy of ~5 eV, were taken into account. Moreover, the lowest 50 singlet and triplet excited states were calculated for each calculated optimized geometry. Notably, our TDDFT calculations do not include spin−orbit coupling, so that singlet−triplet excitations have zero oscillator strengths. To check the effect of solvation on the calculated optical absorption spectra, we performed TDDFT calculations of the low-lying excitations at the singlet optimized geometry, including solvation effects by means of the nonequilibrium implementation of the polarizable continuum model;[32,33] as in the experimental conditions, the chosen solvent was acetonitrile.

(23) Frisch, M. J.; Trucks, G. W.; Schlegel, H. B.; Scuseria, G. E.; Robb, M. A.; Cheeseman, J. R.; Montgomery, J. A., Jr.; Vreven, T.; Kudin, K. N.; Burant, J. C.; Millam, J. M.; Iyengar, S. S.; Tomasi, J.; Barone, V.; Mennucci, B.; Cossi, M.; Scalmani, G.; Rega, N.; Petersson, G. A.; Nakatsuji, H.; Hada, M.; Ehara, M.; Toyota, K.; Fukuda, R.; Hasegawa, J.; Ishida, M.; Nakajima, T.; Honda, Y.; Kitao, O.; Nakai, H.; Klene, M.; Li, X.; Knox, J. E.; Hratchian, H. P.; Cross, J. B.; Bakken, V.; Adamo, C.; Jaramillo, J.; Gomperts, R.; Stratmann, R. E.; Yazyev, O.; Austin, A. J.; Cammi, R.; Pomelli, C.; Ochterski, J. W.; Ayala, P. Y.; Morokuma, K.; Voth, G. A.; Salvador, P.; Dannenberg, J. J.; Zakrzewski, V. G.; Dapprich, S.; Daniels, A. D.; Strain, M. C.; Farkas, O.; Malick, D. K.; Rabuck, A. D.; Raghavachari, K.; Foresman, J. B.; Ortiz, J. V.; Cui, Q.; Baboul, A. G.; Clifford, S.; Cioslowski, J.; Stefanov, B. B.; Liu, G.; Liashenko, A.; Piskorz, P.; Komaromi, I.; Martin, R. L.; Fox, D. J.; Keith, T.; Al-Laham, M. A.; Peng, C. Y.; Nanayakkara, A.; Challacombe, M.; Gill, P. M. W.; Johnson, B.; Chen, W.; Wong, M. W.; Gonzalez, C.; Pople, J. A. *Gaussian 03*, Revision B.05; Gaussian, Inc.: Wallingford, CT, 2004.
(24) Becke, A. D. *J. Chem. Phys.* **1993**, *98*, 5648−5652.
(25) Hay, P. J.; Wadt, W. R. *J. Chem. Phys.* **1985**, *82*, 270.
(26) Wadt, W. R.; Hay, P. J. *J. Chem. Phys.* **1985**, *82*, 284.
(27) (a) Watchers, A. J. H. *J. Chem. Phys.* **1970**, *52*, 1033. (b) Hay, P. J. *J. Chem. Phys.* **1977**, *66*, 4377.
(28) Glukhovstev, M. N.; Pross, A.; McGrath, M. P.; Radom, L. *J. Chem. Phys.* **1995**, *103*, 1878.
(29) Ditchfield, R.; Herhe, W. J.; Pople, J. A. *J. Chem. Phys.* **1971**, *54*, 724.
(30) Sinha, P.; Wilson, A. K.; Omary, M. A. *J. Am. Chem. Soc.* **2005**, *127*, 12488.
(31) EMSL basis set library available at http://www.emsl.pnl.gov/forms/basisform.html.
(32) (a) Miertus, S.; Scrocco, S.; Tomasi, J. *Chem. Phys.* **1981**, *55*, 117. (b) Cossi, M.; Rega, N.; Scalmani, G.; Barone, V. *J. Comput. Chem.* **2003**, *24*, 669.
(33) Cossi, M.; Barone, V. *J. Chem. Phys.* **2001**, *115*, 4708.

Table 1. Main Optimized Geometrical Parameters for the Optimized DFT Structures of $[Cu_4I_4py_4]$ in the S_0, T_1, and T_2 States, Compared to the X-ray Structural Data

parameters	exp[a]	S_0[b]	T_1	T_2
Cu−N, Å	2.02−2.06	2.059 (2.001)	2.029	2.002
Cu−I, Å	2.665−2.734	2.817−2.861 (2.788−2.789)	3.105−2.910	2.818−2.754
Cu−−Cu, Å	2.619−2.722	2.685−2.834 (2.418−2.484)	2.582−2.575	3.002−3.024
I−−I, Å	4.442−4.594	4.681−4.831 (4.698−4.816)	5.464−5.043	4.679−4.528
Cu−N−C, deg	117−124	120.6 (121.1)	120.4	120.8
N−Cu−I, deg	95.2−111.4	102.8−106.2 (98.6−102.4)	99.6−100.9	108.4−110.5
Cu−I−Cu, deg	57.7−61.1	56.9−59.9 (51.4−52.9)	49.2−50.6	64.4−65.7

[a] Reference 2. [b] For the S_0 ground state, data calculated with the larger 6-311G*/6-31G* basis set are also reported in parentheses.

Characterization of the nature of the TDDFT transitions in terms of single orbital excitations is usually possible, provided one has access to the eigenvectors. The latter are made up of two component vectors, X and Y, related to single-particle excitations and de-excitations, respectively. In G03, however, the program provides only the (dominant) components of the sum vector $X + Y$, and it is thus impossible in principle to separate the interfering excitation and de-excitation components. To the extent, however, that we may reasonably assume that the de-excitation vector Y is small compared to X (it would be exactly zero in the Tamm−Dancoff or single-excitation CI approximation), we may take the square of the $X + Y$ vector components as a qualitative measure of the weight pertaining to the corresponding single excitations. For closed-shell molecules, the G03 TDDFT vectors are actually normalized to $^1/_2$ (with the normalization condition $<X - Y|X + Y> = {}^1/_2$), so we take the double of the squared coefficients. The results thus obtained for our calculations are those displayed in Table 2.

Materials and Methods. $[Cu_4I_4py_4]$ was synthesized by adding excess pyridine to a stirred solution of CuI in concentrated aqueous KI. The product precipitated immediately as a white powder, was separated by filtration, and then was washed successively with saturated KI (aqueous) to remove excess CuI, with H_2O to remove KI, with methanol to remove excess ligand, and then with hexanes. The $[Cu_4I_4py_4]$ was recrystallized from dichloromethane/pentane and then dried in vacuo. The yield was quantitative based on the amount of CuI used.

The UV−visible absorption spectra of $[Cu_4I_4py_4]$ in acetonitrile at different concentrations were recorded on a Jasco V-530 double-beam spectrophotometer. The emission spectra of $[Cu_4I_4py_4]$ in toluene solution were recorded on a Jobin Yvonne Fluorolog 3 spectrofluorometer.

Results and Discussion

Optimized Geometries and Electronic Structure of the Ground State and of the Lowest Triplet States. The calculated optimized geometry of the S_0 ground state is reported in Figure 2, together with the geometry of the Cu_4I_4 core for S_0 and for the two lowest triplet states T_1 and T_2. Main optimized geometrical parameters for the three states are compared to the published X-ray data[2] in Table 1, together with results obtained for the S_0 ground state with the larger 6-311G*/6-31G* basis set.

Our calculated geometrical parameters for the ground state are in fair agreement with X-ray experimental data, despite

Table 2. Calculated TDDFT Singlet−Singlet Excitation Energies, Oscillator Strengths, and Composition in Terms of Main Orbital Transitions for the Most Intense ($f > 0.02$) Transitions of $[Cu_4I_4py_4]$[a]

excited state	symmetry	transition wavelength λ, nm	oscillator strength f	nature of the transition
13	B2	367.15	0.0453	61% (HOMO − 3 → LUMO) + 26% (HOMO − 4/HOMO − 5 → LUMO + 2/LUMO + 3)
14	E	366.68	0.0498	48% (HOMO − 3 → LUMO + 2/LUMO + 3) + 25% (HOMO − 5/HOMO − 4 → LUMO) + 12% (HOMO − 5/HOMO − 4 → LUMO + 1)
54	B2	321.47	0.1145	88% (HOMO − 3 → LUMO + 8)
55	E	317.28	0.2020	50% (HOMO − 5/HOMO − 4 → LUMO + 8) + 37% (HOMO − 7/HOMO − 6 → LUMO + 8)
80	E	298.57	0.0886	51% (HOMO − 9/HOMO − 8 → LUMO + 1) + 28% (HOMO − 9/HOMO − 8 → LUMO)
84	B2	297.17	0.0630	42% (HOMO − 9 → LUMO + 2) + 42% (HOMO − 8 → LUMO + 3)
115	B2	272.74	0.0212	59% (HOMO − 16 → LUMO) +12% (HOMO − 17 → LUMO +1)

[a] For degenerate E states the oscillator strengths are given by the sum of the intensities of the two partner transitions. See Computational Details section for the definition of the percentages characterizing each transition.

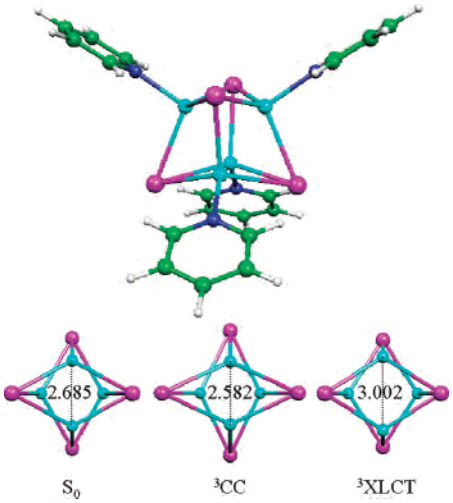

Figure 2. Optimized molecular structures of the S_0, T_1, and T_2 states of the $[Cu_4I_4py_4]$ complex. Cu, cyan; I, purple; N, blue; C, green; H, white. Intradimer Cu−Cu distances (in angstroms) are also reported.

a general small overestimation of bond lengths that can be probably traced back to the lack of polarization functions in the basis set. This discrepancy is quite evident for the nonbonding I−I distances, which are the result of the combination of both Cu−I and Cu−Cu distances. Using the larger 6-311G*/6-31G* basis set does not substantially improve the agreement with experiment for calculated bond distances and angles of ground-state $Cu_4I_4py_4$ in reasonable agreement with those obtained by the LANL2DZ basis set. An exception is represented by the Cu−Cu distances, which were calculated to be considerably shorter with the 6-311G*/6-31G* basis set than found for the LANL2DZ results and experimental data (2.418−2.484 vs 2.685−2.834 and 2.619−2.722 Å for 6-311G*/6-31G*, LANL2DZ, and experimental data, respectively). On the basis of these geometrical data, we used LANL2DZ for geometry optimizations of the two triplet species. The optimized S_0 structure shows a "dimer of dimers" type of arrangement with two equivalent $[Cu_2I_2py_2]$ units, with shorter calculated Cu−Cu distances (2.685 Å) within each equivalent unit and longer interunit parameters (2.834 Å) while Cu−I distances show lower variations among different dimers (Figure 2 and Table 1). This asymmetry in Cu−Cu distances is originated from the D_{2d} symmetry constraints used for geometry optimizations. Frequency calculations performed on the D_{2d}-optimized S_0 structure revealed a small negative frequency (-4.9 cm^{-1}), which disappeared upon lowering the symmetry to C_2. The geometrical rearrangement taking place from D_{2d} to C_2 symmetry, however, was negligible as well as the associated energy gain (0.15 kcal/mol), and the C_2 optimized structure essentially maintained the D_{2d} symmetry, which was therefore retained in all subsequent calculations to exploit the computational savings deriving from the higher symmetry in the subsequent TDDFT calculations.

A schematic representation of the molecular orbitals of the ground state of $[Cu_4I_4py_4]$ for the relevant geometries S_0, T_1, and T_2 is reported in Figure 3, while isodensity surface plots of some relevant selected molecular orbitals calculated at the S_0 geometry are reported in Figure 4. The excited states of both singlet and triplet character are obtained within TDDFT as linear combinations of orbital excitations from the singlet ground state; therefore, in Figure 3 we report the molecular orbitals of the singlet ground state calculated for the optimized geometries of the S_0, T_1, and T_2 states.

At the S_0 state optimized geometry, the 26 highest occupied molecular orbitals (HOMOs) are combinations of copper d and iodine p orbitals, with pyridine-based bonding orbitals lying at lower energies (see Figure 3). Among the occupied states based on copper and iodine orbitals, those belonging to the HOMO/HOMO − 8 set are mainly composed of iodine lone pairs with smaller contributions coming from antibonding copper d_z^2 and nitrogen lone pairs combinations. This orbital set is followed at lower energy by nonbonding copper t_{2g} orbitals (HOMO − 9/HOMO − 11). Still at lower energy, we find various combinations of copper d and iodine p bonding orbitals (HOMO − 12/HOMO − 25). Among this orbital set, we limit our attention to the HOMO − 16, a bonding combination of the four copper d_z^2 orbitals.

The eight lowest unoccupied molecular orbitals (LUMOs) are two groups of almost degenerate π^* orbitals of the pyridine ligands. The lower-lying set has nodes between the nitrogen and the ortho carbons and between the para and meta carbons; the higher-lying set has nodes between the ortho and meta carbons. Above these two pyridine π^* sets, the LUMO + 8 is a combination of copper and iodine s-p states. Notably, this orbital has bonding character among the four Cu atoms and antibonding character between all the Cu

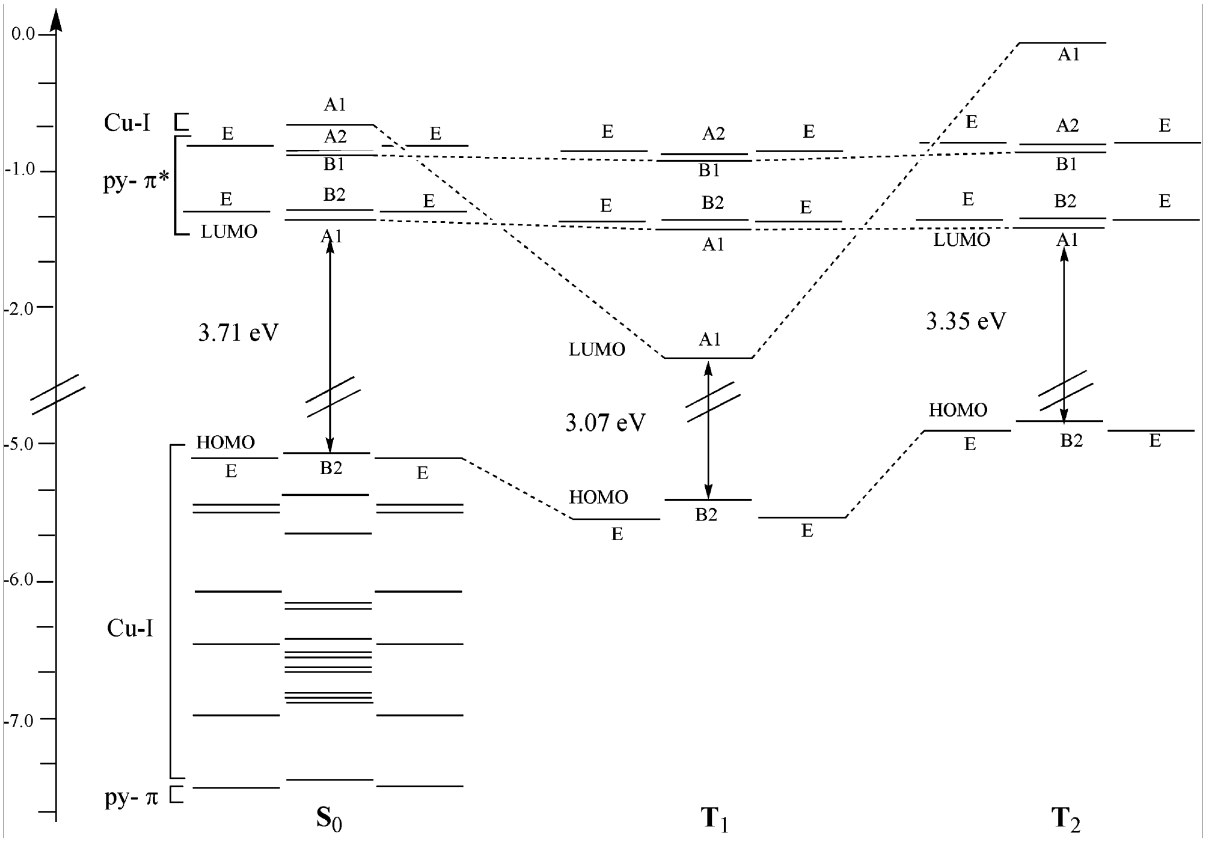

Figure 3. Schematic representation of the molecular orbitals for the singlet ground state calculated at the S_0, T_1, and T_2 optimized geometries. For the T_1 and T_2 geometries, only the relevant HOMOs and LUMOs (and their symmetries) are reported for comparison.

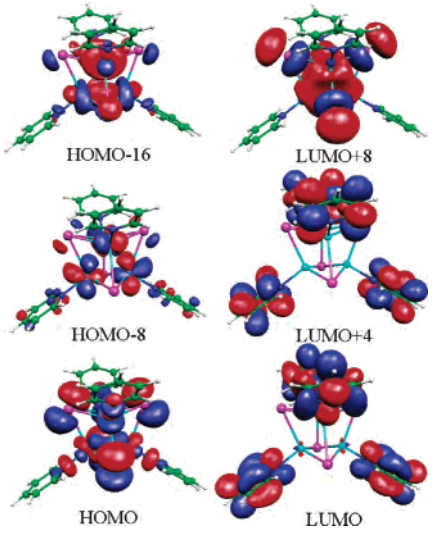

Figure 4. Isodensity surface plots of some relevant molecular orbitals calculated for the singlet ground state at the S_0 optimized geometry.

and I atoms. This electronic structure picture is in agreement with previous theoretical calculations by Vitale et al.,[17,18] apart from the fact that we find pyridine-based bonding orbitals at lower energy. We notice, on the other hand, that recent DFT calculations on the related $[Cu_4I_4(NH_3)_4]$ and $[Cu_4I_4(PH_3)_4]$ systems showed the HOMOs to be made by metal-based orbitals,[19] with halide contributions never exceeding 40%.This might be either an effect of the different ligands or most likely the result of the different exchange-correlation functional used in ref 19, which, compared to the hybrid B3LYP functional used here, does not contain any Hartree−Fock exchange.

Starting from the optimized S_0 geometry and imposing a triplet spin multiplicity, we selectively populated the pyridine π^* LUMO and the Cu−I-based LUMO + 8, both of *A*1 symmetry, allowing the corresponding geometrical structures to relax. We expect the D_{2d} symmetry to be a good approximation for the description of T_1 and T_2 optimized structures, as already found for S_0, since in both cases we populate orbitals of *A*1 symmetry and the resulting states are effectively of *A*1 symmetry. Indeed, no Jahn−Teller distortions of the excited states should take place in this case, as might instead be the case if one would populate doubly degenerate orbitals with *E* symmetry by a single electron. Surprisingly, population of the higher-lying LUMO + 8 was found to lead to the lowest energy triplet state (T_1), which was calculated to lie at 2.52 eV (58.0 kcal/mol) above the ground singlet state optimized geometry, with the triplet state energy obtained by population of the pyridine π^* (T_2) calculated to be 3.17 eV (73.0 kcal/mol) above the ground singlet state optimized geometry. In both cases, the expectation value of S^2 is calculated to be 2.01, confirming that both T_1 and T_2 are pure triplet spin states.

As is clear from the data presented in Table 1 and Figure 2, T_1 shows large geometrical variations with respect to the ground state. The largest variations are within the Cu_4I_4 core: the calculated Cu−I and I−I distances increase while the Cu−Cu distances decrease substantially with respect to the ground state. Smaller <Cu−I−Cu angles are also

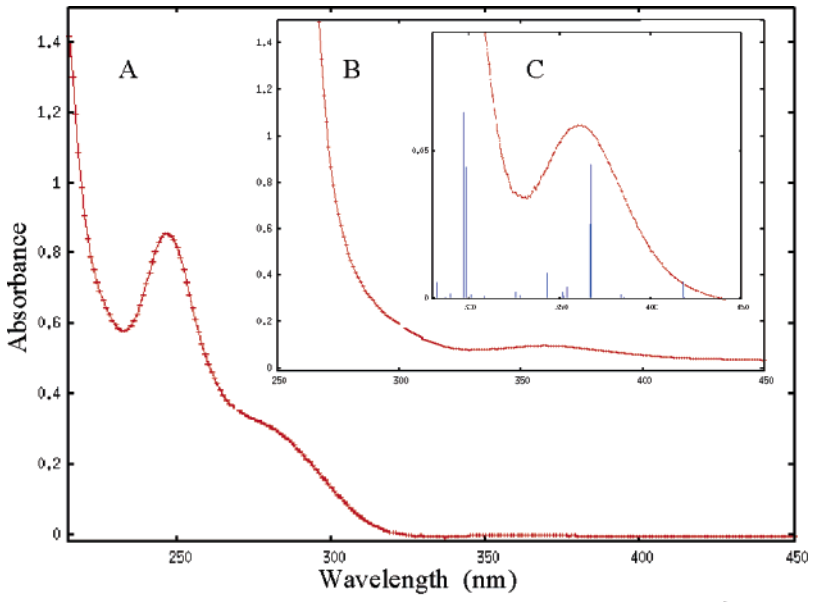

Figure 5. Experimental optical absorption spectra of $[Cu_4I_4py_4]$ in CH_3CN: (A) 5×10^{-6} M, (B) 1×10^{-4} M, and (C) 2.5×10^{-4} M. In panel C, a comparison of the experimental absorption spectrum with calculated excitation energies and oscillator strengths (vertical blue lines) is reported.

calculated, as would be expected from the related bond length changes. On the other hand, only a slight shortening of the Cu−N distances is calculated. Such variation of the geometrical parameters reflects the electron redistribution that occurs upon going from the S_0 ground state to the T_1 state. The one-electron transition is from the HOMO, composed essentially of iodine lone pairs, to the LUMO + 8, which has Cu−I antibonding and Cu−Cu bonding character. We notice that shortening of intramolecular Cu−Cu bond distances in low-lying emitting triplet states of trimeric Cu−pyrazolate complexes has been recently established on experimental[34] and theoretical grounds.[35]

The geometrical rearrangement for the T_2 state is more limited than that for the T_1 state. The Cu−N distances shorten slightly and the Cu−Cu distances lengthen with respect to the optimized structure of the ground state, S_0. The Cu−I and I−I distances are almost unaffected. Mainly as a result of the Cu−I bond lengthening, the <Cu−I−Cu angle is found to increase compared to the S_0 optimized geometry.

The substantial geometrical relaxation occurring on T_1 has a profound impact on the electronic structure. Indeed, if we look at the singlet ground state molecular orbitals calculated at the T_1 optimized geometry (Figure 3), we find the LUMO to be what was the LUMO + 8 for the S_0 optimized geometry, with the two pyridine π^* sets now being the LUMO + 1/LUMO + 8. Notably, for the T_1 geometry, the LUMO is considerably stabilized (by 1.68 eV) with respect to the corresponding orbital (LUMO + 8) calculated for the S_0 structure. Such orbital stabilization is clearly a result of the expansion (contraction) of the I_4 (Cu_4) tetrahedra calculated for the T_1 state—see Table 1 and Figure 3—while the two pyridine π^* sets are almost unaffected by the geometrical change of the cluster core. The HOMO is also stabilized with respect to the S_0 optimized structure (by 0.36 eV), probably reflecting the diminished electrostatic repulsion among the iodine lone pairs due to the considerable increase of the I−I interatomic distances.

For the T_2 optimized geometry, on the other hand, the ordering of the singlet ground state molecular orbitals is qualitatively unchanged with respect to that calculated at the S_0 optimized geometry. The HOMOs are slightly destabilized (by 0.27 eV) by the small decrease of the Cu−N bond lengths, the LUMO/LUMO + 7 pyridine π^* set is almost unaffected, while the LUMO + 8 is destabilized by 0.62 eV as a result of the expansion of the $Cu_4I_4N_4$ core.

Optical Absorption Spectrum. The optical absorption spectra of $[Cu_4I_4py_4]$ in CH_3CN solution at different concentrations are reported in Figure 5. A 247 nm broad absorption band (A in Figure 5) is observed, together with a shoulder at 285 nm, working with a 5×10^{-6} M solution. When the concentration is increased, a much weaker absorption centered at 360 nm becomes evident (B in Figure 5) and is clearly visible in the 2.5×10^{-4} M solution (C in Figure 5).

In order to simulate a large portion of the absorption electronic spectrum of $[Cu_4I_4py_4]$, we calculated the lowest 120 TDDFT singlet excitation energies using the LANL2DZ basis set. Most of the calculated transitions have low or negligible oscillator strength (f) and only those with $f > 0.02$ are reported in Table 2. Comparison of the four lowest singlet−singlet and singlet−triplet excitation energies calculated with the LANL2DZ and 6-311G*/6-31G* basis sets shows that the latter provides excitation energies that are consistently red-shifted by ca. 0.2 eV compared to the former, with a similar pattern of oscillator strengths [2.834, 2.837, 2.837, and 2.837 vs 2.643, 2.643, 2.643, and 2.644 eV, for singlet−triplet transitions with the LANL2DZ and 6-311G*/

(34) Vorontsov, I. I.; Kovalevsky, A. Y.; Chen, Yu.-S.; Graber, T.; Gembicky, M.; Novozhilova, I. V.; Omary, M. A.; Coppens, P. *Phys. Rev. Lett.* **2005**, *94*, 193003.
(35) Grimes, T.; Omary, M. A.; Dias, H. V. R.; Cundari, T. R. *J. Phys. Chem. A* **2006**, *110*, 5823.

Table 3. Calculated TDDFT Lowest CC and XLCT Singlet−Singlet and Singlet−Triplet Excitation Energies of $[Cu_4I_4py_4]$ at the S_0, ^{3}CC, and ^{3}XLCT Optimized Geometries[a]

	energy, eV (wavelength, nm)		
state	S_0	T_1	T_2
S_0	0.000	0.580	0.175
^{1}CC	3.469 (357)	2.294 (540)	3.819 (325)
^{1}XLCT	2.965 (418)	3.300 (376)	2.635 (471)
^{3}CC	3.191 (389)	1.875 (661)	3.703 (335)
^{3}XLCT	2.834 (438)	3.166 (392)	2.504 (495)

[a] Energy differences between the S_0 state at its optimized geometry and at the T_1 and T_2 geometries are also reported.

6-31G* basis sets, respectively, and 2.965 ($f = 0.0002$), 2.965 ($f = 0.0002$), 2.967 ($f = 0.0057$), and 2.971 ($f = 0.0000$) vs 2.761 ($f = 0.0004$), 2.761 ($f = 0.0004$), 2.761 ($f = 0.0000$), and 2.765 ($f = 0.0024$) eV for singlet−singlet transitions with the LANL2DZ and 6-311G*/6-31G* basis sets respectively]. Given the similarity of the results obtained with the two basis sets, we retained the smaller LANL2DZ basis for all subsequent calculations.

The two lowest energy transitions with sizable intensity ($f = 0.0453$ and 0.0498) are calculated at 367 nm. The final states of these transitions are within the lowest π^* LUMOs set, starting from orbitals of the HOMO − 3/HOMO − 5 set, which have their largest components from the iodine lone pairs. These charge-transfer transitions are therefore assigned as ^{1}XLCT absorptions. The calculated wavelength nicely correlates with the presence of the weak absorption band measured at 360 nm in the experimental $[Cu_4I_4py_4]$ absorption spectrum; see C in Figure 5, in which the low-energy portion of the experimental absorption spectrum is compared to the calculated excitation energies and oscillator strengths. Inclusion of solvation effects does not lead to qualitative changes in the low-energy region of the absorption spectrum: four transitions of sizable intensity are calculated at 362.73, 361.58, and 359.53 nm, with oscillator strengths of 0.0057, 2 × 0.0036, and 0.0049, giving rise to the band experimentally found at 360 nm. The most significant changes observed in solution are an overall reduction of the transition intensities and the appearance of a fourth transition of sizable intensity in the low-energy spectral region. Given the qualitative agreement between the calculated data in vacuo and in solution, data in vacuo are discussed hereafter. At higher energy a group of two closely spaced, intense transitions ($f = 0.1145$ and $f = 0.2020$) are calculated to occur at 321 and 317 nm. These transitions involve population of the HOMO + 8, with antibonding Cu−I and bonding Cu−Cu character, while the starting orbitals are within the same HOMO − 3/HOMO − 5 set discussed above. The two transitions have therefore ^{1}CC character and can be related to the absorption band found at 304 nm in the experimental spectrum of $[Cu_4I_4py_4]$ in benzene solution[8] or to the 285 nm shoulder found in acetonitrile solution, Figure 5. Most notably, the intense ^{1}XLCT and ^{1}CC features calculated at 367 and 321−317 nm are in good agreement with the excitation spectra obtained by monitoring the HE and LE emissions,[8] showing excitation maxima in toluene solution at room temperature at 352 and 325 nm, respectively. Below

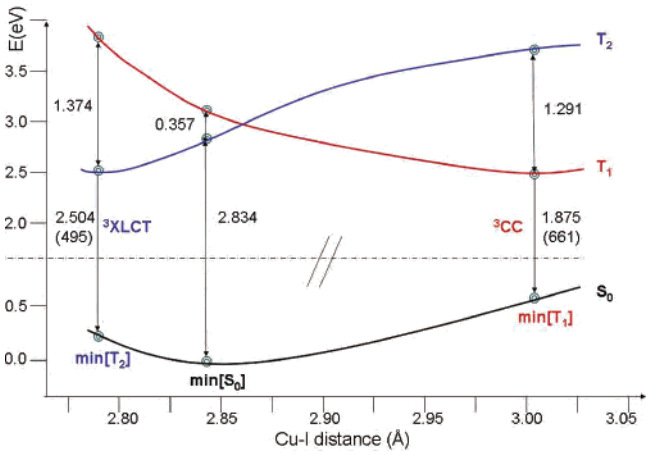

Figure 6. Calculated singlet−triplet TDDFT excitation energies plotted against the Cu−I distance for the S_0, T_1, and T_2 optimized structures. Also marked on the S_0 potential energy curve are the minima corresponding to the S_0, T_1, and T_2 optimized structures. Data in parentheses are wavelengths in nanometers.

300 nm we calculated three transitions of sizable intensity ($f = 0.0886$, 0.0630, and 0.0212) at 299, 297, and 273 nm, respectively. The transitions at 299 and 297 nm have as starting states the HOMO − 9/HOMO − 11 copper t_{2g} set, while the 273 nm transition has the HOMO − 16, of copper d_z^2 character as starting state. These three transitions have as final states the lowest π^* LUMOs set and therefore can be assigned as metal-to-ligand charge-transfer (^{1}MLCT) excitations. These transitions are most likely related to the 285 nm shoulder found in the experimental spectrum.

Triplet Excited States: Emission. A comparison of the lowest TDDFT singlet and triplet excited states of $[Cu_4I_4py_4]$ calculated at the S_0, T_1, and T_2 optimized geometries is reported in Table 3. The lowest triplet excited-state energies calculated for the T_1 and T_2 optimized geometries give some insight into the nature of the emitting states, while the singlet excited states are reported for comparison. Moreover, it is interesting to use the singlet−triplet TDDFT excited-state energies calculated at the S_0, T_1, and T_2 optimized geometries to draw a schematic representation of the potential energy surfaces involved in the dual emission of $[Cu_4I_4py_4]$. In doing so, one needs to select a distortion coordinate that characterizes the geometrical arrangement of the three minima (S_0, T_1, and T_2) related to the emission process. In particular, we chose to plot the excited-state energies as a function of the average Cu−I distances: this necessarily arbitrary choice is dictated by the fact that this parameter reflects to some extent the expansion−contraction of the cubane core and shows sizable variations on going from the S_0 to the T_1 and T_2 minima. The results are reported in Figure 6.

At the S_0 optimized geometry, the lowest singlet excited state, calculated at 2.965 eV (418 nm) above the ground state, corresponds to a weak transition of ^{1}XLCT character ($f = 0.0002$) while the lowest ^{1}CC state is the 21st singlet excited state calculated at 3.469 eV (357 nm) ($f = 0.0007$). The lowest triplet state is of ^{3}XLCT character and is calculated at 2.834 eV (438 nm) above the ground state, while the lowest ^{3}CC is the ninth excited triplet state and is calculated at 3.191 eV (389 nm). Therefore at the S_0 optimized

geometry the order of the XLCT and CC states is the same for both singlet and triplet excited states, with triplet excited states, as expected, at lower energy. We also notice that at the S_0 optimized geometry the ^{3}XLCT and ^{3}CC are separated by only 0.357 eV, while a larger separation (0.504 eV) is calculated between the ^{1}XLCT and ^{1}CC excited states.

This picture changes dramatically upon moving to the T_1 optimized geometry. In this case, the lowest triplet excited state originates from a single HOMO−LUMO transition calculated at 1.875 eV (661 nm). The corresponding ΔSCF value, obtained from the difference between the triplet and singlet SCF energies at the T_1 optimized geometry, is 1.936 eV (640 nm), therefore comparable to the TDDFT value (they differ by only 0.061 eV). These values are in excellent agreement with the experimental LE emission at 1.797 eV (690 nm) measured at room temperature in toluene solution. Having in mind the electronic structure discussed above, the lowest triplet excited state is readily assigned as ^{3}CC, which has its origin in excitation from the iodine lone pairs to the Cu−Cu bonding/Cu−I antibonding LUMO. The corresponding ^{1}CC state is calculated at 2.294 eV (540 nm) ($f = 0.0103$), while the lowest ^{3}XLCT is calculated to be the 16th triplet excitation, lying at 3.166 eV (392 nm). We notice that, compared to the S_0 geometry, the ^{3}XLCT and ^{3}CC are now well separated in energy (by 1.291 eV; see Figure 6).

For the optimized T_2 geometry, the lowest triplet state is of ^{3}XLCT character and is calculated at 2.504 eV (495 nm), again in excellent agreement with the experimental HE emission found at room temperature in toluene solution at 2.695 eV (460 nm). The corresponding ^{1}XLCT state is calculated at 2.635 eV (417 nm), while singlet and triplet CC states were calculated at 325 and 335 nm, respectively. The corresponding ΔSCF value is calculated to be 2.991 eV, in fair agreement with the lowest TDDFT singlet−triplet excitation. We finally notice that the joint absorption and emission calculated data are in agreement with the experimental excitation spectra obtained by monitoring the two emission features, showing a reversed order of excitation spectra in which the HE and LE emissions correspond to LE and HE excitations, respectively.[8]

Conclusions

The results of the DFT/TDDFT calculations described here have provided a detailed description of the molecular geometries of the $[Cu_4I_4py_4]$ tetranuclear cluster for the S_0, T_1, and T_2 states (ground state and the two lowest triplet excited states). As expected, since the cluster electron core is involved, going from the S_0 to the ^{3}CC state involves a profound deformation of the cluster core geometry with a significant increase of the Cu−I and I−I distances while the Cu−Cu distances decrease together with the <Cu−I−Cu angle. Since the η^1-nitrogen donor pyridine ligand is not involved, the Cu−N distances are not affected.

Much less significant is the deformation going from the S_0 ground-state geometry to that of the T_2 state. In this case the cluster core geometry remains quite unchanged while the Cu−N distances shorten significantly. This would be expected given the more negative character of the η^1-nitrogen donor pyridine ligand in the halide-to-pyridine charge-transfer excited state. The relevant geometrical relaxation of the ^{3}CC state, which is considerably different from that of the ^{3}XLCT state, produces a profound change of the ground-state molecular orbitals in comparison to the S_0 optimized geometry. While at the ground-state geometry the ^{3}XLCT state has a lower energy than the ^{3}CC state, the strong geometrical relaxation on the ^{3}CC state surface leads to a reverse order of the excited states. Such electronic perturbation is the origin of the reverse order of excited states of emission compared to the excitation and reflected in the dual luminescence.

The strong geometrical relaxation of the ^{3}CC state justifies the observed thermochromic and rigidochromic behavior connected with the nuclear motion impediment at low temperature and in rigid matrix. Once the respective excited states have relaxed to their equilibrated geometries, the ^{3}XLCT state is at higher energy than the ^{3}CC state. Although the distortions along different trajectories provide a barrier for interconversion between states, the presence of the lower energy ^{3}CC state provides an additional channel for deactivation of the higher energy ^{3}XLCT state in ambient temperature solutions.[8] This may explain the much longer lifetime of the LE emission compared to the HE one in solution, although it should be emphasized that the lifetimes of the two emissions are comparable in 77 K glassy solutions.

Our calculations, which provide a unified picture of the stationary points on the excited states potential energy surfaces, produce a calculated dual emission spectrum in excellent agreement with available experimental values and confirm the earlier, qualitative assignments of the emission bands.[1,7,8,11−16] Furthermore, the calculated electronic absorption spectrum, which involves evaluation of singlet excited states, is in good agreement with the experimental one. In particular, for the first time we have been able to identify the higher energy absorption bands as having MLCT character, while the absorption bands at lower energy are related to charge-transfer processes of ^{1}CC and ^{1}XLCT character, respectively, thus involving the cluster core and the bridging iodines.

In conclusion, our calculations not only have confirmed the involvement of ^{3}CC and ^{3}XLCT excited states as origin of the dual emission but also have shown unequivocally the great sensitivity of the electronic structure to involvement of the cluster core in the excited states. The orbitals of the pyridine ligand, which are the most stable among the HOMO and LUMO orbitals, are much less affected by the involvement not only of cluster core but also of their bonding to the cluster core in the excited states. Owing to the excellent agreement of the experimental data with our theoretical approach to this class of Cu(I) compounds, we are now extending this kind of calculations to other geometrical arrangements of Cu(I) compounds, like polymeric stair or single chains, which still lack an acceptable definition of their electronic structure and therefore of the origin of the transitions involved in absorption and emission spectra.

Acknowledgment. We thank F. Tarantelli for helpful discussions. F.D.A., S.F., A.S., E.C., and R.U. thank MIUR for financial support (FIRB 2003: Molecular compounds and hybrid nanostructured materials with resonant and non resonant optical properties for photonic devices). P.C.F. thanks the U.S. National Science Foundation for support.

IC061147F